Nitric oxide selectively suppresses I_H currents mediated by HCN1 containing channels

Cornelia Kopp-Scheinpflug[1], Beatrice M. Pigott[2] and Ian D. Forsythe[2]

[1] Division of Neurobiology, Department Biology II, Ludwig-Maximilians-University Munich, Großhadernerstr. 2, 82152 Planegg-Martinsried, Germany.
[2] Department of Cell Physiology and Pharmacology, University of Leicester, Leicester. LE1 9HN UK.

Key Words: HCN1, HCN2, neuronal nitric oxide synthase (nNOS), auditory brainstem, MNTB, LSO, MSO, SPN

Corresponding author: Ian D. Forsythe, Department of Cell Physiology & Pharmacology, Medical Sciences Building, University of Leicester, LE1 9HN, UK
Telephone: +44 (0) 116 252 5580
Fax: +44 (0) 116 252 5616
E-mail: idf@le.ac.uk

Short title: NO suppresses HCN1

Figures: 8
Abstract: 241 words
Introduction: 447 words
Discussion: 1697 words

Acknowledgements: This work was funded by the Medical Research Council (MRC, MR/K005170/1) and Deutsche Forschungsgemeinschaft (DFG, KO2207/3-1). We are grateful to Matt Nolan (Edinburgh University, UK) for sharing the HCN1 knockout mice with us and to Olga Alexandrowa (Ludwig-Maximilians-University Munich, Germany) for sharing her expertise with cell reconstruction.

Author contributions:
CKS conducted electrophysiological experiments and analysed data. BP performed immunohistochemistry. CKS and IDF jointly conceived the project and wrote the manuscript.

Key Points:

- The superior olivary complex (SOC) exhibits a spectrum of HCN1 and HCN2 subunit expression, which generate I_H currents with fast and slow kinetics, respectively.
- Neuronal nitric oxide synthase (nNOS) was broadly distributed across the SOC.
- NO hyperpolarizes the half-activation voltage of HCN1-mediated currents and caused a slowing of the I_H current kinetics in the respective nuclei (MSO, LSO and SPN). This signalling was independent of cGMP.
- NO also caused a depolarizing shift in the half-activation voltage of HCN2-mediated I_H currents, increasing activation at resting potentials; this was cGMP-dependent.
- Thus NO-signalling suppressed fast HCN1-mediated currents and potentiated slow HCN2-mediated currents, modulating the overall kinetics and magnitude of the endogenous I_H.

ABSTRACT

Hyperpolarization-activated non-specific cation permeable channels (HCN) mediate I_H currents which are modulated by cGMP, cAMP and by nitric oxide (NO) signalling. Channel properties depend upon subunit composition (HCN1-4 and accessory subunits) as demonstrated in expression systems, however physiological relevance requires investigation in native neurons with intact intracellular signalling. Here we use the superior olivary complex (SOC), which exhibits a distinctive pattern of HCN1 and HCN2 expression, to investigate NO modulation of the respective I_H currents, and compare properties in wild type and HCN1 knockout mice. The medial nucleus of the trapezoid body (MNTB) expresses HCN2 subunits exclusively, and sends inhibitory projections to the medial and lateral superior olives (MSO, LSO) and the superior paraolivary nucleus (SPN). In contrast to the MNTB, these target nuclei possess an I_H with fast kinetics, and express HCN1 subunits. NO is generated in the SOC following synaptic activity and here we show that NO selectively suppresses HCN1, while enhancing I_H mediated by HCN2 subunits. NO hyperpolarizes the half-activation of HCN1-mediated currents and slows the kinetics of native I_H currents in the MSO, LSO and SPN. This modulation was independent of cGMP and absent in transgenic mice lacking HCN1. Independently, NO signalling depolarizes the half-activation of HCN2-mediated I_H currents in a cGMP-dependent manner. Thus NO selectively suppresses fast HCN1-mediated I_H and facilitates a slow HCN2-mediated I_H, so generating a spectrum of modulation, dependent on the local expression of HCN1 and/or HCN2 and the actions of NO signalling.

INTRODUCTION

Hyperpolarization-activated cyclic nucleotide modulated channel (HCN) subunits are encoded by the HCN1-4 gene family and form the molecular substrate of I_H currents that regulate resting membrane potential and excitability in the brain and heart (Santoro *et al.*, 1998; Robinson & Siegelbaum, 2003; Wahl-Schott & Biel, 2009). Each HCN channel is formed by a tetrameric complex of subunits with both homo- and heteromeric channels being suggested (Biel *et al.*, 2009). All four subunits are expressed in the brain, but studies show that they differ in activation kinetics (HCN1: fast, HCN2: intermediate, HCN3&4: slow), voltage-dependent activation (half-activation voltages for

HCN1: -70mV, HCN2: -95mV, HCN3: -85mV, HCN4: -100mV) and the depolarizing shift in activation voltage mediated by cyclic nucleotide modulation (HCN2&4: most sensitive, HCN1&3: less sensitive) (Robinson & Siegelbaum, 2003; Biel *et al.*, 2009; Wahl-Schott & Biel, 2009; Shah, 2014). These findings are mainly based on research using cell expression systems, but there is increasing evidence that site-specific accessory subunits, local kinase and/or phosphatase activity also contribute to shaping the characteristics of I_H currents in native neurons (Santoro *et al.*, 2009; Wahl-Schott & Biel, 2009). It is therefore essential to study HCN kinetics and modulation in native neurons with intact intracellular signalling.

Throughout the nervous system, synaptic activity can generate nitric oxide (NO). This messenger molecule is involved in the regulation of synaptic transmission and neuronal function (Garthwaite, 2008; Steinert *et al.*, 2008; Steinert *et al.*, 2011; Hardingham *et al.*, 2013) through binding of NO to its receptor, guanylyl cyclase (sGC), and subsequent production of cGMP. NO-cGMP signalling could regulate native HCN-mediated currents directly through changes in cGMP concentrations, or indirectly through effects on cGMP-dependent protein kinases or phosphodiesterases. Cyclic nucleotides (cAMP, cGMP) and NO modulate HCN channel activity in many brain areas (Pape & Mager, 1992; Ingram & Williams, 1996; Garthwaite *et al.*, 2006; Wilson & Garthwaite, 2010; Neitz *et al.*, 2011; Neitz *et al.*, 2013). The medial nucleus of the trapezoid body (MNTB) expresses exclusively HCN2 and sends inhibitory projections to the HCN1 expressing medial and lateral superior olives (MSO, LSO), and to the superior paraolivary nucleus (SPN) which expresses both HCN1 and HCN2 subunits. We seek to examine HCN subunit-specific roles in neuronal signalling by exploiting the distinctive patterns of HCN1 and HCN2 expression across the superior olivary complex (SOC) (Koch *et al.*, 2004). The large amplitude of I_H currents (surpassing those of CA1 neurons by 10-fold) increases the reliability of observing modulatory effects, and use of HCN1-KO mice allowed differentiation between NO modulation of HCN1 and HCN2 subunits.

The results show that NO suppresses HCN1-mediated I_H currents by a guanylyl cyclase independent negative shift in the voltage-dependence of activation; and simultaneously facilitates HCN2-dominated I_H currents by a GC-dependent positive shift in activation. For neurons that express both HCN1 and HCN2, the net effect is to slow I_H kinetics and increase the I_H contribution to resting

conductances, thereby depolarizing the resting membrane potential and reducing the peak conductance activated by hyperpolarization.

METHODS

Brain slice preparation. Experiments were carried out in accordance with the UK Animals (Scientific Procedures) Act 1986 and as revised by European Directive 2010/63/EU. The HCN1-KO mice (obtained from Edinburgh University) were backcrossed onto a CBA/Ca background. CBA/Ca and HCN1-KO mice (P13-P21) of either sex that were killed by decapitation and brainstem slices containing the superior olivary complex were prepared. As described previously (Johnston *et al.*, 2008), transverse slices were cut in an ice-cold (< 4°C) low sodium artificial CSF, incubated at ~37°C for 1 hour in normal aCSF, and then stored at room temperature (~20°C) in a continually recycling slice-maintenance chamber until transferred to the slice rig at 37°C for recording. The normal aCSF comprised (in mM): NaCl 125, KCl 2.5, $NaHCO_3$ 26, glucose 10, NaH_2PO_4 1.25, sodium pyruvate 2, myo-inositol 3, $CaCl_2$ 2, $MgCl_2$ 1 and ascorbic acid 0.5; pH was 7.4 when continuously bubbled with 95% O_2/5% CO_2. In the low sodium aCSF, NaCl was replaced by 250 mM sucrose and $CaCl_2$ and $MgCl_2$ concentrations were 0.1 and 4 mM, respectively. All chemicals were obtained from Sigma, unless otherwise noted.

Electrophysiology. A slice was transferred to a Peltier-controlled recording chamber (37±1°C) on the stage of a Nikon FN600 microscope (Nikon, Tokyo, Japan). Individual cells were visualized using differential interference contrast (DIC) optics and 63× (0.9 NA) water immersion objectives. Whole-cell patch-clamp recordings were made using a Multiclamp 700B amplifier (Molecular Devices, Sunnyvale, CA, USA) and pClamp 10 software (Molecular Devices), sampling at 50 kHz and filtering at 10 kHz. Patch pipettes were pulled from filamented borosilicate glass (GC150F-7.5, Harvard Apparatus, Edenbridge, UK) using a 2-stage vertical puller (PC-10 Narishige, Tokyo, Japan) and filled with a solution containing (mM): KGluconate 97.5, KCl 32.5, HEPES 40, EGTA 5, $MgCl_2$ 1, Na_2phosphocreatine 5, pH was adjusted to 7.2 with KOH. Final resistances were 3-4 MΩ. Whole-cell

access resistances were <10 MΩ and series resistances were routinely compensated by 70%. All voltages were corrected for an 11mV liquid junction potential.

The amplitudes of the I_H currents were measured during a hyperpolarizing voltage command as the difference between the instantaneous current and the sustained currents. Activation kinetics of I_H were voltage-dependent, and fitted by a double exponential function, dominated by the fast component. Activation in the HCN1-KO was much slower and was well fit by a single exponential function with similar values to the slow time constant of the wild-type data. Voltage-dependent half-activation was determined by fitting a Boltzmann function to the plot of the conductance ratio (G/Gmax) vs. the applied voltage.

Immunohistochemistry. Methods were adapted from Kopp-Scheinpflug *et al.* (2011). Briefly, male or female adult mice (P30-60) wild-type or neuronal nitric oxide synthase knockout mice (nNOS-KO, lacking exon 6) (Gyurko *et al.*, 2002) on a CBA/Ca background, were decapitated and their brainstems rapidly frozen in Lamb OCT embedding matrix (ThermoFisher Scientific, Waltham, MA, USA). Transverse, 12 µm-thick tissue sections were prepared on Menzel-Gläser Polysine slides using a cryostat (Microm HM 560; both ThermoFisher Scientific). For HCN1 and HCN2 labelling, sections were fixed in 4 % PFA diluted in PBS (25 min at 4 ˚C). Sections to be stained for nNOS were exposed to 99.8 % methanol (10 min, -20 ˚C) instead of PFA since this procedure was found to yield superior antibody specificity in separate experiments (unpublished data). Sections were then washed for 5 min, 3 times in PBS containing 0.1 % triton X-100 (PBS-T) and blocked in PBS-T plus 1 % BSA and 10 % normal goat serum (1 h at room temperature; serum concentrations were tripled for nNOS staining; Vector Labs, Burlingame, CA, USA). Washes with PBS-T were repeated and the antibodies for nNOS (1:1000; SC-648, Santa Cruz; Dallas, TX, USA), HCN1 (1:500; APC-056, Alomone, Jerusalem, Israel) or HCN2 (1:1000; APC-030, Alomone) diluted in blocking solution, were applied for 18-20 h at 4 ˚C in a humid environment. Control sections for the selectivity of the secondary antibodies received blocking solution minus antisera. Sections were then washed for 10 min, 3 times in PBS-T and incubated with Alexa Fluor 488 goat anti-rabbit IgG (1:1000 in blocking solution; Life Technologies, Carlsbad, CA, USA) for 1 h at room temperature in the dark. Washes were repeated and sections were counterstained (DAPI, Vector Labs), mounted and photographed using a Leica DM2500

fluorescence microscope (Leica, Wetzlar, Germany. Photographs are representative of data from at least 2 sections from each of 3 animals. Experimental and control sections were prepared, stained and photographed in parallel and while the experimenter was blinded to genotype. Control and experimental photos were adjusted equally for brightness and contrast using Adobe Photoshop (Adobe, Mountain View, CA, USA).

Statistics. Statistical analyses were performed with SigmaPlot/SigmaStat/™ (SPSS Science, Chicago, IL). Individual data points represent the data collected from single neurons and bar graphs mean values ± standard error of the mean (S.E.M.). Values of *n* indicate the number of neurons, which were from at least 3 different animals. Statistical comparisons between multiple different data sets were made using one-way repeated measures analysis of variance (ANOVA). For data following non-normal distributions, significance was assessed using the Kruskal-Wallis ANOVA on ranks test. Differences between just two data sets in a classical before/after treatment were assessed by Students t-test (normal distribution) or Mann-Whitney Rank Sum Test. Normality was evaluated by the Shapiro-Wilk test. Differences were considered statistically significant when $p<0.05$ (***: $p\leq0.001$; **: $p\leq0.01$; *: $p\leq0.05$).

RESULTS

Mouse SOC neurons express HCN1, HCN2 and nNOS.

The SOC includes the medial nucleus trapezoid body (MNTB) and its target nuclei, the medial and lateral superior olives (MSO and LSO) and the SPN. Immunohistochemistry for HCN1 and HCN2 in the mouse SOC revealed a distinct distribution for each subunit that was consistent with the kinetics of I_H measured in each nucleus and previous findings about the distribution of HCN1 and HCN2 in the rat (Koch *et al.* 2004). HCN1 immunofluorescence (green in Fig. 1A) was intense in cell bodies and fibres that were predominant in those nuclei with the fastest I_H (MSO and LSO), moderate in SPN and absent where I_H exhibits slow kinetics (MNTB). The specificity of this immunofluorescence for HCN1 was verified previously using HCN1 knockout tissue (Kopp-Scheinpflug *et al.* 2011). In contrast to the HCN1 antibody, the HCN2 antibody, which generates comparable labelling in wild-type and HCN1 knockout tissue (Kopp-Scheinpflug *et al.* 2011) strongly stained MNTB neuron soma (Fig. 1B). The

LSO and SPN were also immunopositive for HCN2, but unlike in the MNTB, HCN2 labelling in LSO and SPN was concentrated in the neuropil (Figs. B_i and B_{iii}). No expression of HCN3 or HCN4 was observed in SOC neurons, while some minor staining of HCN4 was observed in axonal tracts (data not shown). Overall this is consistent with immunohistochemical localization in the rat (Koch *et al.*, 2004; Notomi & Shigemoto, 2004) and the focus of this paper on somatic currents mediated by HCN1 and HCN2.

-Insert Figure 1 about here-

In neurons, NO is generated by nNOS and consistent with previous findings in hamster (Reuss *et al.*, 2000), gerbil and mouse (Yassin *et al.*, 2014), immunofluorescence for nNOS was observed in neuronal soma throughout the MNTB and SPN, as well as in fibres and neuropil throughout MNTB, SPN, MSO and LSO (Fig. 2A). The specificity of the antibody staining for nNOS was validated here by the absence of immunostaining in tissue from nNOS-KO mice (Fig. 2B).

-Insert Figure 2 about here-

NO modulates ionic conductances in SOC neurons without changing the overall firing pattern.

MNTB neurons send inhibitory projections to the LSO, the MSO and the SPN. In the target neurons this inhibition hyperpolarizes the membrane and activates I_H. MNTB neurons are also known to generate NO upon synaptic activity (Steinert *et al.*, 2008). To investigate the effect of NO on I_H in each nucleus, whole-cell patch-clamp recordings were obtained from neurons of the mouse SOC before and during bath application of an NO-donor (SNP, 100µM). In response to 200ms depolarising current injections (Fig. 3A, black traces) all SOC neurons responded with one or more action potentials according to their established firing properties (Brew & Forsythe, 1995; Barnes-Davies *et al.*, 2004; Scott *et al.*, 2005; Felix *et al.*, 2011; Kopp-Scheinpflug *et al.*, 2011). The response to sustained outward current injections (200ms duration) shows a rapid initial hyperpolarization, followed by the classic 'sag' in membrane potential that is indicative of the presence of I_H (Fig. 3A,

blue traces). In contrast to the large sag observed in MSO and LSO neurons, in SPN neurons the sag was more moderate and of slower time-course, while MNTB neurons exhibited the slowest and smallest amplitude sag. The ratio between the peak hyperpolarisation and the membrane potential after 100ms (R1, Fig. 3A top left) and 200ms (R2, Fig. 3A top left) has been used to quantify the sag and evaluate the contribution of HCN1- vs. HCN2-mediated currents to I_H (Nolan *et al.*, 2007). A large difference between R1 and R2 indicates a more slowly activating I_H conductance, such as those dominated by HCN2 subunits. In contrast, when the membrane potential quickly relaxes back to more depolarized values, it reflects I_H with more rapid kinetics as expected for the HCN1-dominated currents of the MSO, LSO and the SPN. In agreement with our immunohistochemical evidence (Fig. 1), a between-group comparison of the HCN1 contribution based on ΔR2-R1 between the four nuclei revealed that MSO (0.010 ±0.002; n=9), LSO (0.013 ±0.002; n=10) and SPN (0.019 ±0.003; n=24) are all significantly different (smaller) from MNTB (0.033 ±0.002; n=15; $p \leq 0.001$), but showed no significant differences between each other (p=0.105; Fig. 3B)

An initial estimation of the degree to which HCN channels were affected by NO was achieved by monitoring current-clamp changes in the voltage sag before (Fig. 3C, grey traces) and during NO exposure (Fig. 3C, blue traces). Activation of nitrergic signalling reduced the magnitude and slowed the time-course of the 'sag' in MSO, LSO and SPN neurons (Fig. 3C) but not in MNTB neurons. Following NO exposure the R-ratios were now similar across all four nuclei (MSO: 0.021 ±0.004, *n*=5; LSO: 0.019 ±0.004, *n*=5; SPN: 0.025 ±0.005, *n*=9; MNTB: 0.028 ±0.004, *n*=4; *p*=0.705; Fig. 3D) implying NO-mediated suppression of a fast HCN1-mediated component in the MSO, LSO and SPN.

-Insert Figure 3 about here-

NO hyperpolarizes I_H half-activation and slows its kinetics to values observed in HCN1-KO.

In order to test the hypothesis that NO selectively supresses HCN1-mediated currents, we focused on MSO neurones, which show a strong HCN1 contribution (Fig 3) and compared these data with I_H measurements from HCN1-KO mice. Under voltage-clamp, control MSO I_H currents activated quickly upon hyperpolarization to voltages only slightly negative to the resting membrane potential (Fig. 4A, B). While maximum I_H conductance was significantly reduced in MSO neurons of HCN1-KO mice,

application of the NO donor SNP caused no significant change in conductance (G_{max} control: 21.6 ±1.1nS, *n*=40; G_{max} HCN1-KO: 7.65 ±1.4nS, *n*=9; G_{max} NO: 17.6 ±2.1nS, *n*=13; $p<0.001$; Fig. 4E). We controlled for rundown over time, with recordings made over a 25 min time-course, that showed no significant change in half-activation voltage.

-Insert Figure 4 about here-

The fast activation time-constant of I_H under control conditions is indicative of a strong contribution of HCN1 subunits in the MSO, corroborating our immunohistochemical results (Fig. 1). The suppression of this fast I_H by NO exposure suggests a mechanism specific for HCN1; and this hypothesis was tested by comparing MSO I_H $V_{1/2}$ and *tau* between wild-type and HCN1 knockout mice (Fig. 4 C-F). The positive half-activation voltage of control (WT) MSO I_H currents ($V_{1/2}$: -83.5 ±1.1mV, *n*=40) was shifted in the hyperpolarizing direction by deletion of HCN1 subunits in HCN1-KO ($V_{1/2}$: -111.3 ±3.3mV, *n*=9; $p\leq0.001$, Fig. 4C, D) or NO signalling in WT MSO neurons ($V_{1/2}$: -107.8 ±3.9mV, *n*=13, Fig. 4C, D). The inward current that remained following NO application was tested for its sensitivity to the I_H blocker ZD7288. A concentration of 20µM ZD7288 blocked 85.5 ±5.1% (n=3) of the remaining current, confirming that although this current had slower kinetics, it was an I_H current. Together these results are consistent with the hypothesis that NO signalling suppresses activation of an HCN1-mediated I_H current by inducing a leftward shift of the activation curve. The absence (HCN1-KO) or reduction of HCN1 contribution (NO exposure) led to slower activation time constants compared to wild-type MSO currents ($\tau_{wild\ type}$: 19.1 ±0.8ms, *n*=40; τ_{HCN1KO}: 168.3 ±14.4ms, *n*=9; τ_{NO}: 36.9 ±4.4ms, *n*=13; $p\leq0.001$; Fig. 4F).

-Insert Figure 5 about here-

NO depolarizes activation of HCN2-mediated currents in a cGMP-dependent manner.

MNTB neurons are characterized by exclusive HCN2 expression (Fig. 1), consistent with the slow sag in membrane potential during hyperpolarisation (Fig. 3). Voltage-clamp recordings of MNTB neurons exhibited further characteristics of HCN2-like I_H currents, including slow activation kinetics of 50.8 ±2.8ms (*n*=25) and hyperpolarized half-activation voltages of -97.68±0.68mV (*n*=25; Fig. 6 B,

C). The absence of HCN1 from MNTB neurons was reinforced by a comparison of I_H currents between wild type and HCN1-KO MNTB neurons which revealed no significant differences in activation voltage ($V_{1/2wild\ type}$: -96.2 ±1.2mV, *n*=25; $V_{1/2HCN1\ KO}$: -97.3 ±4.6, *n*=6; *p*=0.991), activation kinetics ($\tau_{wild\ type}$: 50.8 ±2.8ms, *n*=25; $\tau_{HCN1\ KO}$: 60.6 ±7.2ms, *n*=6; *p*=0.240) or overall conductance ($G_{wild\ type}$: 4.7 ±0.3nS, *n*=25; $G_{HCN1\ KO}$: 4.8 ±.5nS, *n*=6; *p*=0.856; Fig. 6 C-F).

In contrast to the suppression of HCN1-mediated I_H currents in the MSO, NO caused a depolarising shift in the activation voltage in the MNTB ($V_{1/2\ NO}$: -89.3 ±0.9mV, *n*=6; $p \leq 0.05$; Fig. 6 B, C, E) and no change in the activation kinetics (τ_{NO}: 61.3 ±3.1ms, *n*=6; *p*=0.097; Fig. 6 A, F). This depolarizing shift was mimicked by adding 1mM cGMP or cAMP to the intracellular patch solution ($V_{1/2\ cGMP}$: -88.0 ±3.5mV, *n*=6; *p*=1.000; $V_{1/2\ cAMP}$: -82.6 ±3.1mV, *n*=7; *p*=0.275; Fig. 6 G, H), suggesting involvement of the classical NO/cGMP pathway.

-Insert Figure 6 about here-

NO suppresses HCN1-mediated I_H despite co-expression of HCN2

The finding that NO hyperpolarized the $V_{1/2}$ of HCN1 channels (Fig. 4) but depolarized the $V_{1/2}$ of HCN2 currents (Fig. 6) prompted the question: how does NO modulate I_H currents in neurons that express both HCN1 and HCN2 subunits? Neurons in the SPN and LSO express both HCN1 and HCN2 subunits (Fig. 1) and display significantly hyperpolarized resting membrane potentials in HCN1-KO mice ($SPN_{wild\ type}$: -54.2 ±1.4mV, *n*=11; $SPN_{HCN1\ knockout}$: -63.4 ±1.1mV, *n*=11; $p \leq 0.001$; $LSO_{wild\ type}$: -60.6 ±1.5mV, *n*=16; $LSO_{HCN1\ knockout}$: -70.0 ±0.9mV, *n*=4; *p*=0.005), consistent with the idea that both HCN1 and HCN2 channels contribute to I_H currents in these nuclei (Fig. 7). The half-activation voltage for I_H was significantly more hyperpolarized in SPN neurons of HCN1 knockout mice compared to wild type ($V_{1/2wild\ type}$: -87.9 ±0.6mV, *n*=60; $V_{1/2HCN1\ KO}$: -96.6 ±1.6, *n*=11; $p \leq 0.001$; Fig. 7 A, B) and became comparable to that of MNTB neurons, suggesting that the remaining I_H current was now dominated by HCN2. The NO donor, SNP, mimicked the effect of HCN1-KO ($V_{1/2\ NO}$: -102.2 ±2.7, *n*=12), suggesting that NO suppresses HCN1-mediated currents despite the co-expression of HCN2 in the same neurons (Fig. 7A, B). The absence (HCN1-KO) or reduction of HCN1 contribution

(NO exposure) both led to slower activation time constants of SPN I_H currents (τ_{wt}: 30.7 ±1.6ms, *n*=60; τ_{HCN1KO}: 134.3 ±11.7ms, *n*=11; τ_{NO}: 48.2 ±5.4ms, *n*=12; $p \leq 0.001$; Fig. 7D). In SPN neurons from HCN1-KO mice the HCN conductance was significantly reduced, while NO-exposure shifted the activation voltage without significantly changing the conductance ($G_{wild\ type}$: 23.2 ±1.2nS, *n*=60; $G_{HCN1\ KO}$: 10.7 ±2.6nS, *n*=11; G_{NO}: 17.4 ±2.3nS, *n*=12; $p \leq 0.001$; Fig. 7C). The same pattern of results was observed for LSO I_H currents (Fig. 7 E-H).

-Insert Figure 7 about here-

Our data suggest that NO modulation of HCN2 channels is mediated via activation of NO-targeted guanylyl cyclase followed by generation of cGMP (Fig. 6). To test whether HCN1 was also modulated by the NO/cGMP pathway, ODQ (1μM) was used to block the NO receptor in the experiments prior to and during NO application. ODQ did not prevent the hyperpolarization of the half-activation of HCN1-mediated I_H currents in the MSO ($V_{1/2\ ODQ/NO}$: -93.3 ±4.3, *n*=7; Fig. 8 C) or of HCN1/HCN2 mixed currents in the SPN ($V_{1/2\ ODQ/NO}$: -91.6 ±2.7, *n*=7; Fig. 8 A, B, D), suggesting that NO was acting by a cGMP-independent mechanism. This finding was corroborated by the observation that raising intracellular cGMP could not mimic the NO-induced hyperpolarized shift in the activation of HCN1-dominated I_H currents (Fig. 8 C, D).

-Insert Figure 8 about here-

NO hyperpolarized the resting membrane potential (RMP), consistent with a HCN1-mediated I_H contribution to the RMP of the SPN, MSO and LSO, but did not effect the RMP of MNTB neurons (Fig. 9A). The current threshold for AP generation was significantly lower in the MSO (but was unchanged elsewhere, Fig. 9B). Action potential firing at threshold in response to depolarizing current injection was unchanged, but rebound firing following hyperpolarizing current steps was reduced in the SPN (Fig. 9D) during NO perfusion.

We conclude that NO exerts subunit-specific modulation of HCN1 and HCN2 channels by acting through cGMP -independent and -dependent mechanisms respectively, thereby providing a graded modulation of I_H to slow membrane time-constants and hence increased temporal integration.

Insert Figure 9 around here -

DISCUSSION

We have exploited the differences in endogenous expression between nuclei of the SOC to examine the subunit-specific signalling modulation of native I_H currents by NO. HCN1 and HCN2 subunits are expressed widely in the central nervous system (Shah, 2014; He et al., 2014). HCN1 is highly expressed in specific neuron types in cortex, cerebellum, hippocampus and brainstem (Moosmang *et al.*, 1999; Koch *et al.*, 2004) and HCN1-dominated currents have fast kinetics, are active at resting membrane potentials and often found in fast-spiking interneurons. In contrast, HCN2-mediated I_H currents activate more slowly and at more negative voltages (Santoro *et al.*, 2000; Aponte *et al.*, 2006; Wahl-Schott & Biel, 2009) so contributing less to resting conductances. Here we argue that the presence of HCN1 subunits provides an opportunity for activity-dependent suppression of I_H currents via NO signalling. In contrast, the slower HCN2-dominated I_H currents are enhanced by NO. Downstream of NO, HCN1-mediated currents are suppressed in a cGMP-independent manner while HCN2-mediated currents are enhanced via the NO-receptive guanylyl cyclase/cGMP pathway.

Modulation of HCN1

A major function of HCN1 channels is to increase membrane conductance and thereby accelerate or control the membrane time constant in a localised region of a neuron (Pape & McCormick, 1989; Maccaferri & McBain, 1996; Gasparini & DiFrancesco, 1997; Kopp-Scheinpflug *et al.*, 2011). HCN1 channels are abundantly expressed in hippocampal and cortical pyramidal neuron dendrites where they serve to dampen excitability around threshold and modulate the propagation and integration of synaptic potentials, especially those originating from remote sites (Magee, 1998). In cerebellar Purkinje neurons conditional deletion of HCN1 decreased I_H currents and slowed the recovery of the membrane potential following IPSP trains, without changing EPSP kinetics (Rinaldi *et al.*, 2013). This is consistent with a role for HCN1 in regulating integration at hyperpolarized potentials, be that mediated by IPSPs or by hyperpolarising after-potentials (AHP). If HCN1 is suppressed (e.g. by NO),

the balance between IPSP and EPSP integration would favour inhibition, which switches from phasic to tonic and the recovery of the membrane potential after an action potential would be prolonged. This could contribute to mechanisms of anaesthetics such as propofol, isoflurane and halothane which have been reported to suppress HCN1-containing channels (Chen *et al.*, 2005a; Chen *et al.*, 2005b; Chen *et al.*, 2009).

The modulation of HCN1 by NO observed here, was independent of the classic NO/cGMP pathway. Other mechanisms for regulation of HCN1 could involve channel auxiliary subunits, such as Trip8b, which regulates the trafficking of HCN1 channels (Santoro *et al.*, 2009) and acts to hyperpolarize the channel's half-activation voltage. Trip8b reduces the depolarizing effect of cAMP on I_H activation, consistent with the modest effects of cAMP seen here in the MSO, LSO and SPN neurons (Santoro *et al.*, 2009; Hu *et al.*, 2013). Trip8b possesses several potential serine/threonine phosphorylation sites (Santoro *et al.*, 2009) where protein kinase C (PKC) has the potential to phosphorylate and suggests interaction of PKC and NO signalling via s-nitrosylation (Gopalakrishna *et al.*, 1993) which would be independent of cGMP.

Modulation of HCN2

I_H currents with slow kinetics, such as in MNTB or in neurons of the deep cerebellar nucleus (DCN), activate at rather negative voltages and are modulated by cAMP, indicative of HCN2 (Banks *et al.*, 1993; Chen *et al.*, 2005b). HCN2 channels are also sensitive to cGMP, raising the potential for their modulation by an NO/guanylyl cyclase-coupled mechanism (Wilson & Garthwaite, 2010). ATP is typically included in patch solutions, which as suggested by Wilson and Garthwaite (2010) could inhibit NO-activated guanylyl cyclase activity (Roy *et al.*, 2008). We did not add ATP to the intracellular patch pipette solution and we could observe NO/cGMP mediated modulation of the HCN2 dominated I_H in MNTB neurons. Consistent with this result, cGMP-dependent depolarization of I_H activation was reversed when the NO-cGMP pathway was disrupted in guanylyl cyclase (NO receptor) knockout mice, resulting in more negative activation voltages (Neitz *et al.*, 2011; Neitz *et al.*, 2013).

Functional Consequences of I_H modulation

NO is generated in neurones by nNOS upon glutamatergic synaptic transmission (Garthwaite, 2008; Steinert *et al.*, 2008; Steinert *et al.*, 2011; Hardingham *et al.*, 2013). We have shown that NO signalling can activate or suppress I_H currents by cGMP-dependent or -independent mechanisms contingent on the channel subunit composition: HCN1-mediated currents are suppressed by NO, while HCN2-mediated currents are enhanced by NO. cGMP-independent mechanisms of I_H modulation have been observed previously in hypoglossal motoneurons (Wenker et al., 2012).

nNOS is associated with postsynaptic densities (Brenman *et al.*, 1996) and is widely distributed in the brain, as are HCN1 and HCN2 subunits (Notomi & Shigemoto, 2004). The localisation of HCN1 and HCN2 to somatic, dendritic or even axonal and synaptic compartments is highly controlled (Cuttle *et al.*, 2001; Huang *et al.*, 2012; Shah, 2014; Huang & Trussell, 2014) and the ability of I_H to increase or decrease neuronal excitability strongly depends on their subcellular location. At dendritic locations, where nNOS resides, local I_H currents regulate the membrane time constant and thereby control temporal summation, while somatic I_H depolarizes the resting membrane potential and determines threshold for action potential firing (Magee, 1999; Poolos, 2010; Shah, 2014). Dendritic I_H stabilizes the integrative properties of the neurons to ensure an input/output function that is independent from the cells' previous firing activity (Nolan *et al.*, 2003). However, activity-dependent firing is important to establish different forms of plasticity. I_H tunes this equilibrium: activation renders the neuron less dependent on firing history while suppression enables plasticity; such that for example, the loss of dendritic I_H currents in hippocampal CA1 neurons or cerebellar Purkinje neurons causes enhanced stability of place fields (Giocomo *et al.*, 2011; Hussaini *et al.*, 2011). Suppression of I_H currents, as occurs during prolonged synaptic stimulation, will produce a net hyperpolarization that can reduce dendritic filtering, remove location-dependent variability in temporal integration and thereby enhance synchronization of firing across neuronal populations (Magee, 1999, 2000). Facilitation of spatial learning and memory via suppression of HCN1 (Nolan *et al.*, 2004) has not been linked to a physiological signalling cascade, but the results reported here suggest the hypothesis that NO-mediated suppression of HCN1 could fulfil this role.

Differential role of HCN1 versus HCN2 in the auditory nuclei

In auditory brainstem neurons I_H currents are many fold larger in amplitude than elsewhere in the brain (Golding *et al.*, 1999; Koch & Grothe, 2003; Leao *et al.*, 2006; Felix *et al.*, 2011; Kopp-Scheinpflug *et al.*, 2011) and are often paired with low-voltage activated potassium currents (I_{KL}) which mediate an opposing outward current (Cao & Oertel, 2011; Khurana *et al.*, 2011; Golding & Oertel, 2012; Khurana *et al.*, 2012). These two conductances are active at resting membrane potentials, serving to lower input resistances and regulate the threshold and firing patterns of many auditory brainstem neurons. Their action also generates very fast membrane time-constants which limit temporal summation and favour coincidence detection.

In the brainstem of WT CBA/Ca mice neurons possess I_H currents with distinct kinetics (fast and slow). HCN1-KO mice lack a fast kinetic component and the remaining I_H has slow kinetics similar to I_H currents mediated by HCN2 subunits. NO has distinct modulatory actions on these two I_H kinetic components: the first is independent of modulation by cGMP, shifting the fast HCN1 activation to the left (so it is less effectively activated). The second is a cGMP-dependent rightward shift in the activation kinetics of the slow HCN2 dominated I_H. Together these observations are consistent with the hypothesis that native HCN1 channels are homomeric. The I_H current remaining in the HCN1 knockout is consistent with the kinetics of an HCN2 current (perhaps including HCN4 subunits) and suggests the hypothesis that the dual expression and independent differential modulation of HCN1- versus HCN2-containing channels then allows switching between two distinct kinetic forms of the I_H current (fast and slow) rather than formation of heteromeric assemblies with intermediate properties.

If unopposed by I_{KL}, I_H will depolarize the membrane potential and deactivate. In contrast, suppression of I_H currents will produce a net hyperpolarization pushing the membrane potential further from action potential threshold (Liu *et al.*, 2014). Indeed blockade of I_H in auditory neurons causes a reduction in excitability *in vivo* (Shaikh & Finlayson, 2003). In the mammalian auditory system moderate firing rates are able to drive nNOS-positive neurons in the MNTB sufficiently to generate NO, suggesting that NO signalling is active during normal physiology with

increasing importance at more intense stimuli (Steinert *et al.*, 2008; Steinert *et al.*, 2011). In the MNTB, low acoustic background conditions (corresponding to low NO levels) will only activate I_H and I_{KL} during or following an action potential. As the background activity increases, temporal summation will be limited, to ensure typical single action potential responses and entrainment to high stimulus frequencies. Increasing synaptic activity will initiate NO signalling in HCN2-dominated MNTB neurons leading to enhanced I_H currents at resting membrane voltages (see Fig. 6). The I_H-induced depolarisation will recruit I_{KL} at rest so that together the two conductances will decrease the duration of synaptic potentials and guarantee that only large, fast EPSPs will evoke action potentials. NO signalling also shifts the set of potassium conductances available to MNTB neurons from domination by Kv3 to Kv2 channels (Steinert *et al.*, 2011). Kv2.2 currents activate at lower voltages and together with the increased I_H ensure faithful entrainment to high stimulus frequencies especially during periods of high acoustic input (Tong *et al.*, 2013).

In the mouse MSO, HCN1-dominated I_H is large, fast activating and active at rest during low activity conditions when there is presumably little NO signalling and thus comparable with the ventral, high-frequency region of the MSO in gerbils (Baumann *et al.*, 2013). The slower time-course I_H observed in the dorsal part of the gerbil MSO (Baumann *et al.*, 2013) seems at least in part to be carried by HCN4 subunits (Khurana *et al.*, 2012) but HCN4 was not detected in cell bodies of the mouse MSO (unpublished observations). Increasing sound stimulation will trigger NO-signalling in the MSO, LSO and SPN and suppress HCN1-mediated I_H, and this would decrease temporal precision (Khurana *et al.*, 2012). On the other hand, an activity-dependent loss of HCN1 would enhance plasticity as suggested in the hippocampus and entorhinal cortex (Nolan *et al.*, 2004; Giocomo *et al.*, 2011; Hussaini *et al.*, 2011). Overall, increased neuronal firing activity augments the contribution of NO-signalling, which suppresses HCN1-mediated currents and enhances HCN2-mediated currents. With HCN1 current activation shifted to the far left, a depolarizing (rightward) shift of HCN2 currents would cause greater activation at resting membrane potentials and shift overall I_H kinetics from fast to slow. In contrast, reduced acoustic input would cause a rapid decline of NO signalling (Steinert *et al.*, 2011) corroborating findings

that long-term acoustic deprivation (and hence minimal NO signalling) caused an enhancement of HCN1-dominated currents and suppressed HCN2 currents (Hassfurth *et al.*, 2009).

We conclude that NO modulation in the auditory brainstem suppresses the contribution from HCN1-dominated channels and enhances that from HCN2-containing channels. This favors activation of I_H currents with slow kinetics and a more negative voltage-activation. The differential expression of HCN1 (MSO, SPN & LSO) and HCN2 (MNTB, SPN) between the nuclei of the superior olivary complex allows for a spectrum of I_H kinetics (fast to slow) that on activation of NO signalling become dominated by slow kinetics; this phenomenon may underlie activity-dependent control of I_H signalling in many areas of the brain.

FIGURE LEGENDS

Figure 1: Expression of HCN1 and HCN2 within the mouse SOC. A) Intense immunofluorescence for HCN1 (green) was predominant in cell bodies and fibres in the MSO and LSO, sparse in the SPN and absent in the MNTB, where immunofluorescence was of background level. Micrographs taken at high magnification show immunopositive cell soma in the LSO (A_i), MSO (A_{ii}) and SPN (A_{iii}) but MNTB principle neurons showed little or no specific labelling (A_{iv}; HCN1 = green; different sections to A). **B)** HCN2 immunofluorescence (green) was most intense in cell bodies and fibres in the MNTB and SPN, weaker in the LSO and comparable to background in the MSO. **B_{i-iv}**) High magnification images show the presence of immunopositive cell soma in the LSO (B_i), SPN (B_{iii}) and MNTB (B_{iv}) but not MSO (B_{ii}; green = HCN2; different sections to B). Asterisks (*) in B_{iv} mark principal cell bodies. **C)** Control sections for the specificity of the secondary antibody (primary antibodies omitted) showed little non-specific staining (green). Dashed line surrounds MNTB. A, B and C are composites of 2 photographs. Tissue sections shown in A-A_{iv} were adjacent to those shown in B-B_{iv}. Cell nuclei were counterstained with DAPI (blue). Scale bar in A = 150 µM for A, B and C and 25 µM for Ai-iv and Bi-iv.

Figure 2: nNOS immunostaining predominates in the MNTB and SPN. A) Immunofluorescence for nNOS (green) in tissue from a wild type (WT) mouse was apparent in cell

soma, fibers (arrows) and neuropil throughout the MNTB, SPN, MSO and LSO. **B)** Identical staining procedures applied to tissue from a nNOS knockout (KO) showed little or no staining (green), thereby validating the specificity of the immunofluorescence for nNOS in the WT. Inset: secondary antibody control (no primary antibody was used). Image shows MNTB in a knockout section and is representative of the entire SOC. A and B are merged composites of two images to show the full lateral extent of the SOC. Nuclei were counterstained with DAPI (blue). Scale bar = 150 µM applies to both panels and inset.

Figure 3: NO reduces membrane potential sag in MSO, LSO and SPN neurons, but not MNTB neurons. A) Positive current injections depolarized the membrane to AP firing thresholds (MSO: +400pA, LSO: +500pA, SPN: +50pA, MNTB: +250pA). Negative current injections hyperpolarized the membrane to about -100mV (MSO: -600pA, LSO: -800pA, SPN: -600pA, MNTB: -250pA). The sag in membrane potential is indicative of I_H activation. The ratio between the peak hyperpolarization and the membrane potential after 100ms (R1) and after 200ms (R2) was used to evaluate the contribution of HCN1 vs. HCN2 channel subunits. Insets show example neuronal morphology with scale bars of 20µm. **B)** Large differences between R1 and R2 indicate dominance of slow-activating HCN2 subunits, while smaller differences indicate a strong influence of fast activating HCN1 subunits. The median delta (R2-R1) value of the MNTB is statistically significant from the other three nuclei ($p \leq 0.001$; Kruskal-Wallis one-way ANOVA on Ranks). **C)** Application of an NO donor (100µM SNP) reduced the contribution of HCN1 to the restoration of the membrane potential in all nuclei but the MNTB. **D)** Following NO application, there were no significant differences between the four nuclei ($p=0.705$; one-way ANOVA). Summary data are mean ± .S.E.M.; *n*-numbers are indicated by individual data points and the numbers in the bars. Insets: examples of neurons recorded and filled with Lucifer yellow.

Figure 4: NO slows the activation time-constant and hyperpolarizes the half-activation voltage of HCN1-dominated currents. A) Control: fast I_H currents in an MSO cell evoked by step commands from a holding potential of -61mV to -131mV (voltage protocol plotted below). Following application of an NO donor (100µM SNP) I_H currents evoked over the same voltage range were slower to activate (grey traces). Inset: superimposed traces from control (black trace) and following NO

exposure (grey trace) show the slowed I_H activation kinetics. **B)** The voltage dependent activation curve for the cell shown in A was plotted as G/G_{max} and fitted to a Boltzmann equation. **C)** Mean activation curves were plotted from individual cells and fitted to a Boltzmann equation for WT controls (black squares), HCN1 knockout ($HCN1^{KO}$; white squares) and WT following NO exposure (grey circles). **D)** Voltage-dependent half-activation was shifted towards more hyperpolarizing values in $HCN1^{KO}$ mice and following NO-exposure. **E)** In the $HCN1^{KO}$ the HCN conductance was significantly reduced, while NO-exposure shifted the activation voltage without changing the maximum conductance. **F)** The absence ($HCN1^{KO}$) or reduction of HCN1 contribution (NO condition) lead to slower activation time constants of MSO currents. Average data are shown as mean ± S.E.M., Values of *n* are indicated by individual data points and by the number in each bar. ***: $p \leq 0.001$, **: $p \leq 0.01$, *, $p \leq 0.05$. Significance was assessed by one-way ANOVA or Kruskal-Wallis one-way ANOVA on ranks.

Figure 5: No significant changes in amplitude or half-activation voltage of HCN1 currents over 20min. A) Consecutively recorded fast I_H currents in an MSO cell evoked by step commands from a holding potential of -61mV to -131mV. Lower inset shows the instantaneous current (I_{inst}) and the onset of the I_H current. **B)** Mean data showing the amplitudes of the instantaneous current (I_{inst}), the sustained current (I_{sust}) and the difference current (I_H). **C)** Activation curves were plotted for the neuron shown in A) and fitted to a Boltzmann equation (see methods). **D)** Mean data for voltage-dependent half-activation for control recordings and recordings from the same cell 20min later. The range between the dotted lines in D represents the mean ± S.D. of the control $V_{1/2}$ I_H in 40 MSO neurons.

Figure 6: NO depolarizes the half-activation voltage of slow HCN2 channels in a cGMP dependent manner. A) Slow I_H currents in an MNTB neuron evoked by step commands. NO exposure (grey traces) did not change activation kinetics. **B)** Voltage-dependent activation was depolarized during NO exposure in MNTB neurons. **C)** Mean activation curves were plotted from individual cells and fitted to a Boltzmann equation for WT controls (black squares), HCN1 knockout ($HCN1^{KO}$; white squares) and WT following NO exposure (100µM SNP; grey circles). **D)** Mean voltage-dependent activation was more depolarized following NO exposure, but no difference was

found between half-activation voltages of WT and $HCN1^{KO}$ mice. **E+F)** Conductance and activation kinetics were not altered by $HCN1^{KO}$ or NO-exposure. **G)** Mean activation curves for control (black squares), increased intracellular cGMP (1mM; white circles) and increased cAMP (1mM; grey circles). **H)** Increased intracellular cGMP or cAMP mimicked NO-mediated depolarization of half-activation voltages for HCN2 currents. Dotted lines indicate the mean ± S.D. of $V_{1/2}$ during NO application. Average data shown as mean ± S.E.M. N-numbers are indicated by individual data points and by the number in each bar. ***: $p \leq 0.001$, **: $p \leq 0.01$, *, $p \leq 0.05$. Significance was assessed by one-way ANOVA or Kruskal-Wallis one-way ANOVA on Ranks.

Figure 7: NO suppresses HCN1-mediated current in neurons expressing both HCN1 and HCN2 subunits. A) Mean I_H activation curves obtained in the SPN were plotted from individual cells and fitted to a Boltzmann equation for WT controls (black squares), HCN1 knockout ($HCN1^{KO}$; white squares) and WT following NO exposure (100µM SNP ; grey circles). **B)** Voltage-dependent half-activation was hyperpolarized in $HCN1^{KO}$ mice and following NO-exposure in the SPN. **C)** In $HCN1^{KO}$ SPN, the HCN conductance was significantly reduced while NO-exposure did not change the maximum conductance. **D)** The absence ($HCN1^{KO}$) or reduction of HCN1 (NO) led to slower activation time constants of SPN I_H currents. **E-H)** Same design and pattern of results as in A-D but for I_H currents in the LSO. Average data shown as mean ± S.E.M. N-numbers are indicated by individual data points and by the number in each bar. ***: $p \leq 0.001$, **: $p \leq 0.01$, *, $p \leq 0.05$. Significance was assessed by one-way ANOVA or Kruskal-Wallis one-way ANOVA on Ranks.

Figure 8: Modulation of HCN1 is cGMP-independent. A) Fast I_H currents in an SPN cell evoked by step commands from a holding potential of -61mV to -131mV (the voltage protocol is plotted below). Traces were recorded in control (black), in the presence of ODQ alone (1µM, grey, the guanylyl cyclase antagonist) and the red traces were recorded in the presence of ODQ and a NO donor (100µM SNP). **B)** Activation curves were plotted for the neuron shown in A and fitted to a Boltzmann function (see methods) for control (black, square) ODQ alone (grey triangle) and with the NO-donor SNP (red circles). **C, D)** Average data for voltage-dependent half-activation with increased intracellular cGMP (1mM; grey bars), in the presence of ODQ alone (1µM; black bars) and with NO

(100μM SNP; red bars) for cells in the MSO (C) and in the SPN (D). The range between the dotted lines in C and D represents the mean ± S.D. of the control $V_{1/2}$ in the respective nuclei.

Figure 9: Differential expression of HCN subunits between the SOC nuclei underlies differential actions of NO in regulating the RMP and AP threshold. A) Bar graph of mean (± S.E.M.) and individual data points for RMP measured under current clamp in the SPN, MSO, LSO and MNTB in control (filled symbols) and following NO application (open symbols). Only the MNTB showed no significant change. B) Current threshold for triggering an AP was measured as the positive current required to be injected to fire the first AP and was significantly reduced in MSO neurons following NO application. C) The number of APs evoked per trial at the current threshold was not altered following NO application. D) In the SPN, rebound AP firing (inset) triggered on repolarization, following a hyperpolarizing current injection, was reduced following NO application as indicated by the box. ***: $p \leq 0.001$, **: $p \leq 0.01$, *, $p \leq 0.05$. Significance was assessed by Students t-test.

REFERENCES

Aponte Y, Lien CC, Reisinger E & Jonas P. (2006). Hyperpolarization-activated cation channels in fast-spiking interneurons of rat hippocampus. *J Physiol* **574,** 229-243.

Banks MI, Pearce RA & Smith PH. (1993). Hyperpolarization-activated cation current (I_H) in neurons of the medial nucleus of the trapezoid body: voltage-clamp analysis and enhancement by norepinephrine and cAMP suggest a modulatory mechanism in the auditory brainstem. *J Neurophysiol* **70,** 1420-1432.

Barnes-Davies M, Barker MC, Osmani F & Forsythe ID. (2004). Kv1 currents mediate a gradient of principal neuron excitability across the tonotopic axis in the rat lateral superior olive. *Eur J Neurosci* **19,** 325-333.

Baumann VJ, Lehnert S, Leibold C & Koch U. (2013). Tonotopic organization of the hyperpolarization-activated current (I_H) in the mammalian medial superior olive. *Front Neural Circuits* **7,** 117.

Biel M, Wahl-Schott C, Michalakis S & Zong X. (2009). Hyperpolarization-activated cation channels: from genes to function. *Physiol Rev* **89,** 847-885.

Brenman JE, Chao DS, Gee SH, McGee AW, Craven SE, Santillano DR, Wu Z, Huang F, Xia H, Peters MF, Froehner SC & Bredt DS. (1996). Interaction of nitric oxide synthase with the

postsynaptic density protein PSD-95 and alpha1-syntrophin mediated by PDZ domains. *Cell* **84,** 757-767.

Brew HM & Forsythe ID. (1995). Two voltage-dependent K^+ conductances with complementary functions in postsynaptic integration at a central auditory synapse. *J Neurosci* **15,** 8011-8022.

Cao XJ & Oertel D. (2011). The magnitudes of hyperpolarization-activated and low-voltage-activated potassium currents co-vary in neurons of the ventral cochlear nucleus. *J Neurophysiol* **106,** 630-640.

Chen X, Shu S & Bayliss DA. (2005a). Suppression of I_H contributes to propofol-induced inhibition of mouse cortical pyramidal neurons. *J Neurophysiol* **94,** 3872-3883.

Chen X, Shu S, Kennedy DP, Willcox SC & Bayliss DA. (2009). Subunit-specific effects of isoflurane on neuronal I_H in HCN1 knockout mice. *J Neurophysiol* **101,** 129-140.

Chen X, Sirois JE, Lei Q, Talley EM, Lynch C, 3rd & Bayliss DA. (2005b). HCN subunit-specific and cAMP-modulated effects of anesthetics on neuronal pacemaker currents. *J Neurosci* **25,** 5803-5814.

Cuttle MF, Rusznak Z, Wong AY, Owens S & Forsythe ID. (2001). Modulation of a presynaptic hyperpolarization-activated cationic current (I_H) at an excitatory synaptic terminal in the rat auditory brainstem. *J Physiol* **534,** 733-744.

Felix RA, 2nd, Fridberger A, Leijon S, Berrebi AS & Magnusson AK. (2011). Sound rhythms are encoded by postinhibitory rebound spiking in the superior paraolivary nucleus. *J Neurosci* **31,** 12566-12578.

Garthwaite G, Bartus K, Malcolm D, Goodwin D, Kollb-Sielecka M, Dooldeniya C & Garthwaite J. (2006). Signaling from blood vessels to CNS axons through nitric oxide. *J Neurosci* **26,** 7730-7740.

Garthwaite J. (2008). Concepts of neural nitric oxide-mediated transmission. *Eur J Neurosci* **27,** 2783-2802.

Gasparini S & DiFrancesco D. (1997). Action of the hyperpolarization-activated current (I_H) blocker ZD 7288 in hippocampal CA1 neurons. *Pflugers Archiv: Eur J Physiol* **435,** 99-106.

Giocomo LM, Hussaini SA, Zheng F, Kandel ER, Moser MB & Moser EI. (2011). Grid cells use HCN1 channels for spatial scaling. *Cell* **147,** 1159-1170.

Golding NL, Ferragamo MJ & Oertel D. (1999). Role of intrinsic conductances underlying responses to transients in octopus cells of the cochlear nucleus. *J Neurosci* **19,** 2897-2905.

Golding NL & Oertel D. (2012). Synaptic integration in dendrites: exceptional need for speed. *J Physiol* **590,** 5563-5569.

Gopalakrishna R, Chen ZH & Gundimeda U. (1993). Nitric oxide and nitric oxide-generating agents induce a reversible inactivation of protein kinase C activity and phorbol ester binding. *J Biol Chem* **268,** 27180-27185.

Gyurko R, Leupen S & Huang PL. (2002). Deletion of exon 6 of the neuronal nitric oxide synthase gene in mice results in hypogonadism and infertility. *Endocrinology* **143,** 2767-2774.

Hardingham N, Dachtler J & Fox K. (2013). The role of nitric oxide in pre-synaptic plasticity and homeostasis. *Front Cell Neurosci* **7,** 190.

Hassfurth B, Magnusson AK, Grothe B & Koch U. (2009). Sensory deprivation regulates the development of the hyperpolarization-activated current in auditory brainstem neurons. *Eur J Neurosci* **30,** 1227-1238.

He C, Chen F, Li B & Hu Z (2014). Neurophysiology of HCN channels: from cellular functions to multiple regulations. *Prog Neurobiol* **112,** 1–23.

Hu L, Santoro B, Saponaro A, Liu H, Moroni A & Siegelbaum S. (2013). Binding of the auxiliary subunit TRIP8b to HCN channels shifts the mode of action of cAMP. *J Gen Physiol* **142,** 599-612.

Huang H & Trussell LO (2014). Presynaptic HCN channels regulate vesicular glutamate transport. *Neuron* **84,** 340–346.

Huang Z, Lujan R, Martinez-Hernandez J, Lewis AS, Chetkovich DM & Shah MM. (2012). TRIP8b-independent trafficking and plasticity of adult cortical presynaptic HCN1 channels. *J Neurosci* **32,** 14835-14848.

Hussaini SA, Kempadoo KA, Thuault SJ, Siegelbaum SA & Kandel ER. (2011). Increased size and stability of CA1 and CA3 place fields in HCN1 knockout mice. *Neuron* **72,** 643-653.

Ingram SL & Williams JT. (1996). Modulation of the hyperpolarization-activated current (I_H) by cyclic nucleotides in guinea-pig primary afferent neurons. *J Physiol* **492,** 97-106.

Johnston J, Griffin SJ, Baker C, Skrzypiec A, Chernova T & Forsythe ID. (2008). Initial segment Kv2.2 channels mediate a slow delayed rectifier and maintain high frequency action potential firing in medial nucleus of the trapezoid body neurons. *J Physiol* **586,** 3493-3509.

Khurana S, Liu Z, Lewis AS, Rosa K, Chetkovich D & Golding NL. (2012). An essential role for modulation of hyperpolarization-activated current in the development of binaural temporal precision. *J Neurosci* **32,** 2814-2823.

Khurana S, Remme MW, Rinzel J & Golding NL. (2011). Dynamic interaction of Ih and IK-LVA during trains of synaptic potentials in principal neurons of the medial superior olive. *J Neurosci* **31,** 8936-8947.

Koch U, Braun M, Kapfer C & Grothe B. (2004). Distribution of HCN1 and HCN2 in rat auditory brainstem nuclei. *Eur J Neurosci* **20,** 79-91.

Koch U & Grothe B. (2003). Hyperpolarization-activated current (I_H) in the inferior colliculus: distribution and contribution to temporal processing. *J Neurophysiol* **90,** 3679-3687.

Kopp-Scheinpflug C, Tozer AJ, Robinson SW, Tempel BL, Hennig MH & Forsythe ID. (2011). The sound of silence: ionic mechanisms encoding sound termination. *Neuron* **71,** 911-925.

Leao KE, Leao RN, Sun H, Fyffe RE & Walmsley B. (2006). Hyperpolarization-activated currents are differentially expressed in mice brainstem auditory nuclei. *J Physiol* **576,** 849-864.

Liu Q, Lee E & Davis RL. (2014). Heterogeneous intrinsic excitability of murine spiral ganglion neurons is determined by Kv1 and HCN channels. *Neuroscience* **257,** 96-110.

Maccaferri G & McBain CJ. (1996). The hyperpolarization-activated current (I_H) and its contribution to pacemaker activity in rat CA1 hippocampal stratum oriens-alveus interneurones. *J Physiol* **497,** 119-130.

Magee JC. (1998). Dendritic hyperpolarization-activated currents modify the integrative properties of hippocampal CA1 pyramidal neurons. *J Neurosci* **18,** 7613-7624.

Magee JC. (1999). Dendritic l_H normalizes temporal summation in hippocampal CA1 neurons. *Nat Neurosci* **2,** 508-514.

Magee JC. (2000). Dendritic integration of excitatory synaptic input. *Nat Rev Neurosci* **1,** 181-190.

Moosmang S, Biel M, Hofmann F & Ludwig A. (1999). Differential distribution of four hyperpolarization-activated cation channels in mouse brain. *Biol Chem* **380,** 975-980.

Neitz A, Mergia E, Eysel UT, Koesling D & Mittmann T. (2011). Presynaptic nitric oxide/cGMP facilitates glutamate release via hyperpolarization-activated cyclic nucleotide-gated channels in the hippocampus. *Eur J Neurosci* **33,** 1611-1621.

Neitz A, Mergia E, Imbrosci B, Petrasch-Parwez E, Eysel UT, Koesling D & Mittmann T. (2014). Postsynaptic NO/cGMP Increases NMDA Receptor Currents via Hyperpolarization-Activated Cyclic Nucleotide-Gated Channels in the Hippocampus. *Cerebral Cortex **24**, 1923-1936*.

Nolan MF, Dudman JT, Dodson PD & Santoro B. (2007). HCN1 channels control resting and active integrative properties of stellate cells from layer II of the entorhinal cortex. *J Neurosci* **27,** 12440-12451.

Nolan MF, Malleret G, Dudman JT, Buhl DL, Santoro B, Gibbs E, Vronskaya S, Buzsaki G, Siegelbaum SA, Kandel ER & Morozov A. (2004). A behavioral role for dendritic integration:

HCN1 channels constrain spatial memory and plasticity at inputs to distal dendrites of CA1 pyramidal neurons. *Cell* **119,** 719-732.

Nolan MF, Malleret G, Lee KH, Gibbs E, Dudman JT, Santoro B, Yin D, Thompson RF, Siegelbaum SA, Kandel ER & Morozov A. (2003). The hyperpolarization-activated HCN1 channel is important for motor learning and neuronal integration by cerebellar Purkinje cells. *Cell* **115,** 551-564.

Notomi T & Shigemoto R. (2004). Immunohistochemical localization of I_H channel subunits, HCN1-4, in the rat brain. *J Comp Neurol* **471,** 241-276.

Pape HC & Mager R. (1992). Nitric oxide controls oscillatory activity in thalamocortical neurons. *Neuron* **9,** 441-448.

Pape HC & McCormick DA. (1989). Noradrenaline and serotonin selectively modulate thalamic burst firing by enhancing a hyperpolarization-activated cation current. *Nature* **340,** 715-718.

Poolos NP. (2010). Genetic loss of HCN1 channels is exciting, but is it epileptic? *Epilepsy Curr* **10,** 49-51.

Reuss S, Schaeffer DF, Laages MH & Riemann R. (2000). Evidence for increased nitric oxide production in the auditory brainstem of the aged dwarf hamster (Phodopus sungorus): an NADPH-diaphorase histochemical study. *Mech Ageing & Dev* **112,** 125-134.

Rinaldi A, Defterali C, Mialot A, Garden DL, Beraneck M & Nolan MF. (2013). HCN1 channels in cerebellar Purkinje cells promote late stages of learning and constrain synaptic inhibition. *J Physiol* **591,** 5691-5709.

Robinson RB & Siegelbaum SA. (2003). Hyperpolarization-activated cation currents: from molecules to physiological function. *Ann Rev Physiol* **65,** 453-480.

Roy B, Halvey EJ & Garthwaite J. (2008). An enzyme-linked receptor mechanism for nitric oxide-activated guanylyl cyclase. *J Biol Chem* **283,** 18841-18851.

Santoro B, Chen S, Luthi A, Pavlidis P, Shumyatsky GP, Tibbs GR & Siegelbaum SA. (2000). Molecular and functional heterogeneity of hyperpolarization-activated pacemaker channels in the mouse CNS. *J Neurosci* **20,** 5264-5275.

Santoro B, Liu DT, Yao H, Bartsch D, Kandel ER, Siegelbaum SA & Tibbs GR. (1998). Identification of a gene encoding a hyperpolarization-activated pacemaker channel of brain. *Cell* **93,** 717-729.

Santoro B, Piskorowski RA, Pian P, Hu L, Liu H & Siegelbaum SA. (2009). TRIP8b splice variants form a family of auxiliary subunits that regulate gating and trafficking of HCN channels in the brain. *Neuron* **62,** 802-813.

Scott LL, Mathews PJ & Golding NL. (2005). Post-hearing developmental refinement of temporal processing in principal neurons of the medial superior olive. *J Neurosci* **25,** 7887-7895.

Shah MM. (2014). Cortical HCN channels: function, trafficking and plasticity. *J Physiol*, In Press.

Shaikh AG & Finlayson PG. (2003). Hyperpolarization-activated (I_H) conductances affect brainstem auditory neuron excitability. *Hearing Res* **183,** 126-136.

Steinert JR, Kopp-Scheinpflug C, Baker C, Challiss RA, Mistry R, Haustein MD, Griffin SJ, Tong H, Graham BP & Forsythe ID. (2008). Nitric oxide is a volume transmitter regulating postsynaptic excitability at a glutamatergic synapse. *Neuron* **60,** 642-656.

Steinert JR, Robinson SW, Tong H, Haustein MD, Kopp-Scheinpflug C & Forsythe ID. (2011). Nitric oxide is an activity-dependent regulator of target neuron intrinsic excitability. *Neuron* **71,** 291-305.

Tong H, Kopp-Scheinpflug C, Pilati N, Robinson SW, Sinclair JL, Steinert JR, Barnes-Davies M, Allfree R, Grubb BD, Young SM, Jr. & Forsythe ID. (2013). Protection from Noise-Induced Hearing Loss by Kv2.2 Potassium Currents in the Central Medial Olivocochlear System. *J Neurosci* **33,** 9113-9121.

Wahl-Schott C & Biel M. (2009). HCN channels: structure, cellular regulation and physiological function. *Cell & Mol Life Sci* **66,** 470-494.

Wilson GW & Garthwaite J. (2010). Hyperpolarization-activated ion channels as targets for nitric oxide signalling in deep cerebellar nuclei. *Eur J Neurosci* **31,** 1935-1945.

Yassin L, Radtke-Schuller S, Asraf H, Grothe B, Hershfinkel M, Forsythe ID & Kopp-Scheinpflug C. (2014). Nitric oxide signalling modulates synaptic inhibition in the superior paraolivary nucleus (SPN) via cGMP-dependent suppression of KCC2. *Front Neural Circuits* **8**, 65.

Additional Information

None of the authors has any conflicts of interest, beyond the acknowledgment that IDF is a Senior Editor for the Journal of Physiology.

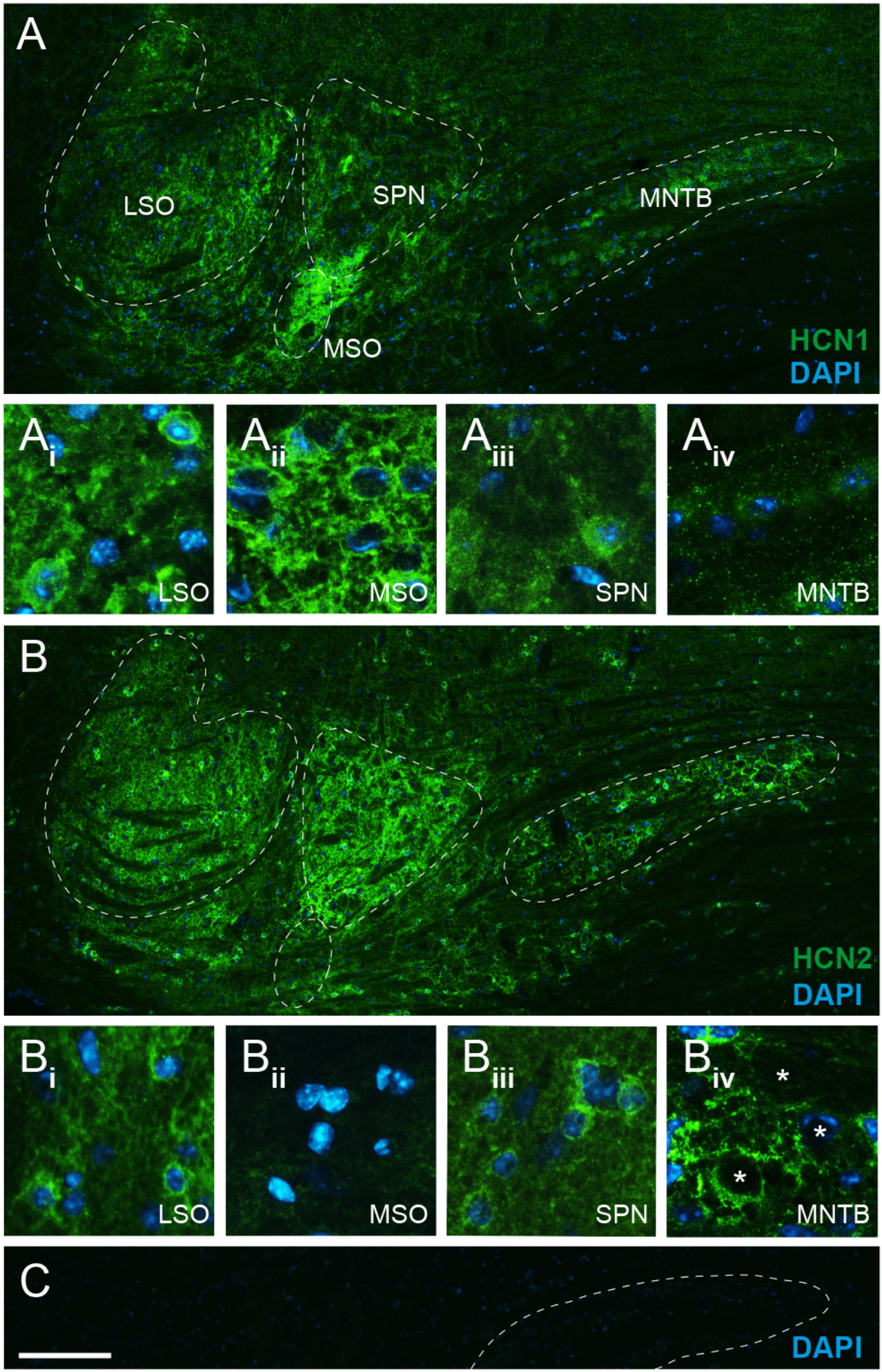
A
LSO
SPN
MNTB
MSO
HCN1
DAPI
A i
LSO
A ii
MSO
A iii
SPN
A iv
MNTB
B
HCN2
DAPI
B i
LSO
B ii
MSO
B iii
SPN
B iv
*
*
*
MNTB
C
DAPI

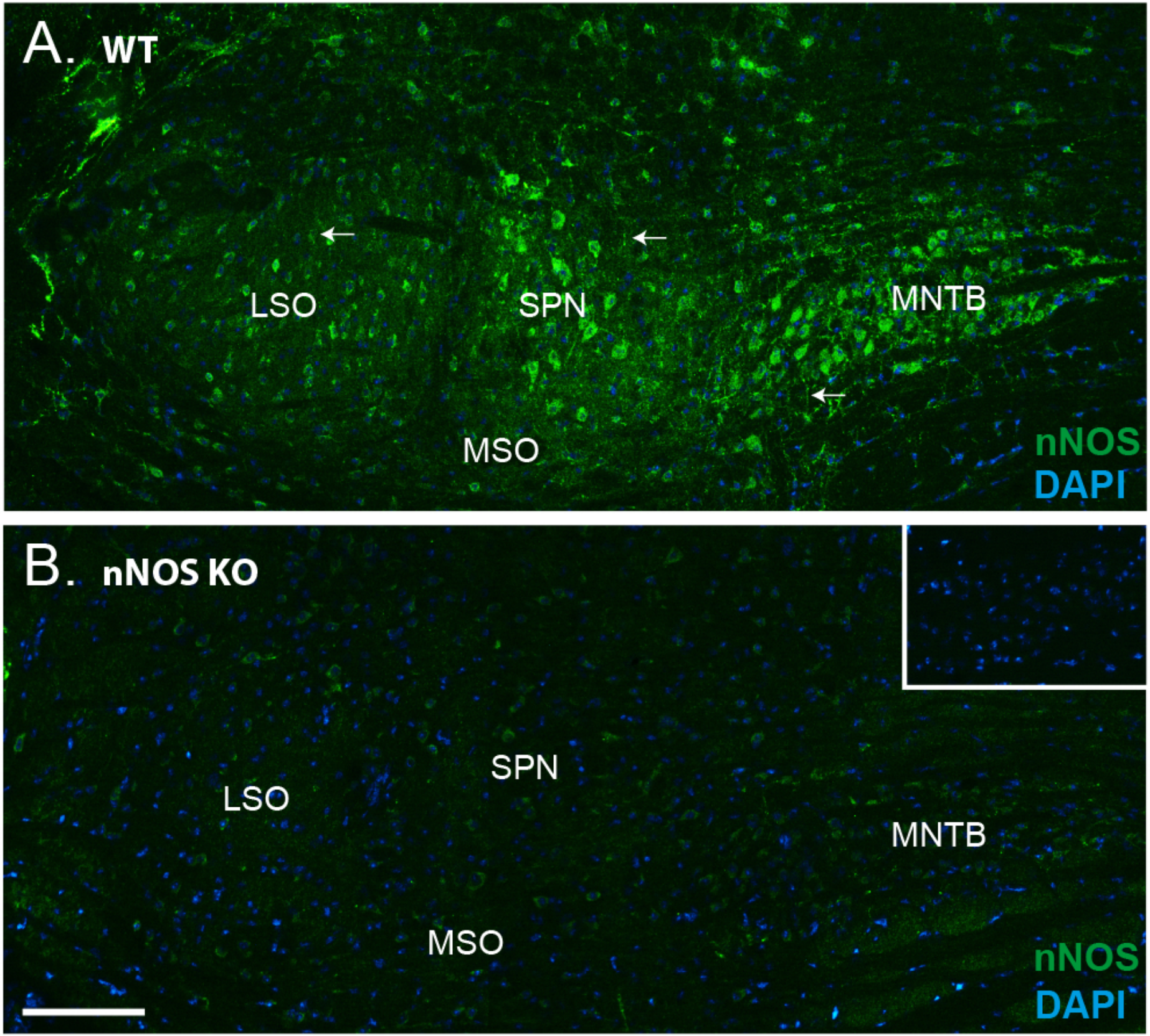
A. WT
LSO
SPN
MNTB
MSO
nNOS
DAPI
B. nNOS KO
LSO
SPN
MNTB
MSO
nNOS
DAPI

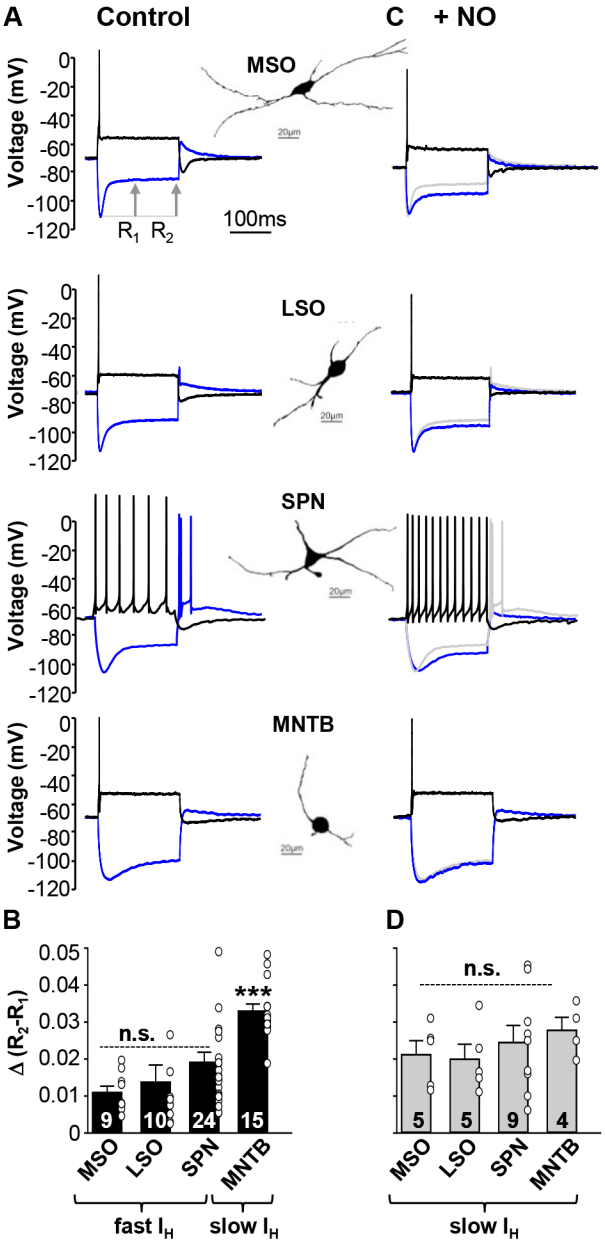
A
Control
C
+ NO
MSO
LSO
SPN
MNTB
Voltage (mV)
0
-20
-40
-60
-80
-100
-120
R1 R2
100ms
20μm
B
D
Δ (R2-R1)
0.05
0.04
0.03
0.02
0.01
0
n.s.
***
9
10
24
15
5
5
9
4
MSO
LSO
SPN
MNTB
fast IH
slow IH
slow IH

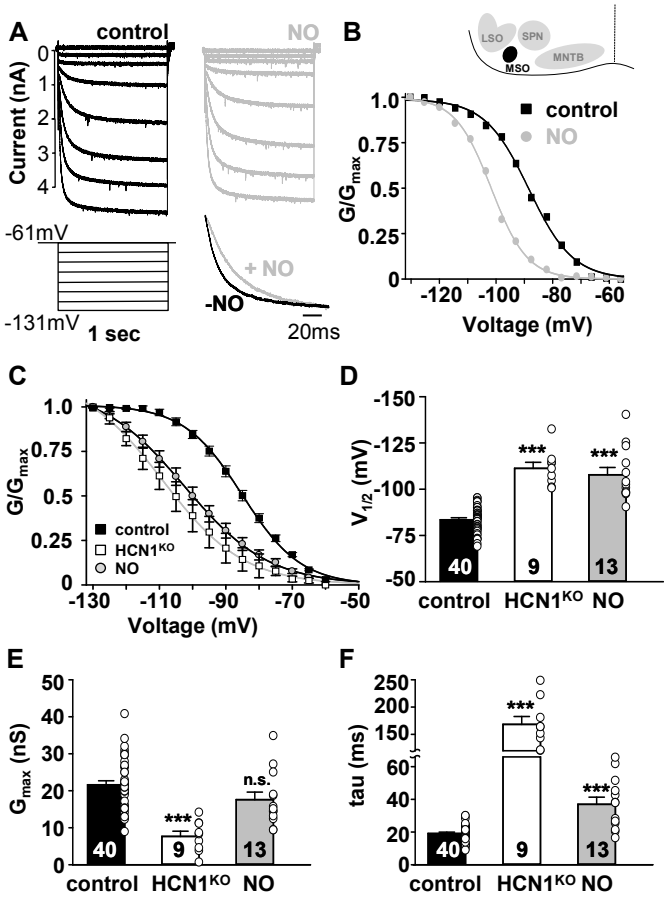
A
control
NO
Current (nA)
0
1
2
3
4
-61mV
-131mV
1 sec
+ NO
-NO
20ms
B
LSO
SPN
MNTB
MSO
control
NO
G/Gmax
1.0
0.75
0.5
0.25
0
-120
-100
-80
-60
Voltage (mV)
C
G/Gmax
control
HCN1KO
NO
-130
-110
-90
-70
-50
Voltage (mV)
D
V1/2 (mV)
-150
-125
-100
-75
-50
***
***
40
9
13
control
HCN1KO
NO
E
Gmax (nS)
50
40
30
20
10
0
***
n.s.
40
9
13
control
HCN1KO
NO
F
tau (ms)
250
200
150
60
40
20
0
***
***
40
9
13
control
HCN1KO
NO

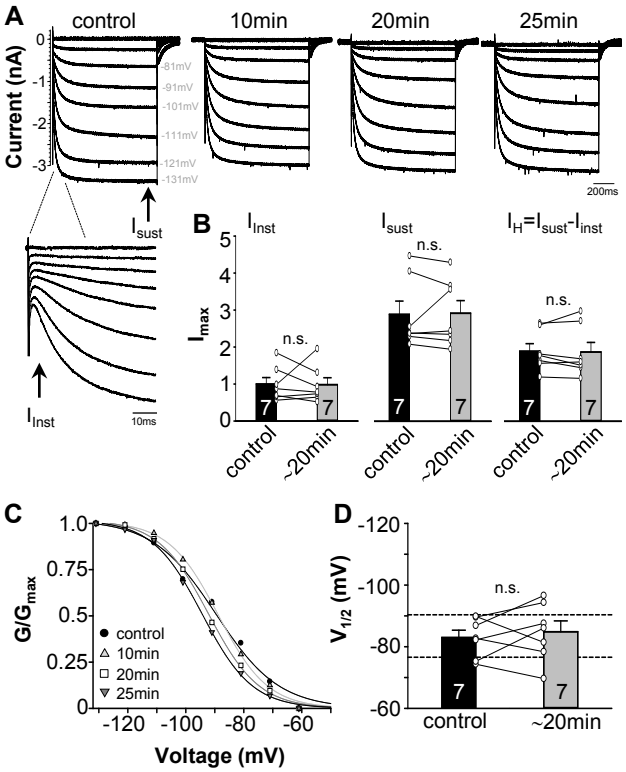
A
control
10min
20min
25min
Current (nA)
0
-1
-2
-3
-81mV
-91mV
-101mV
-111mV
-121mV
-131mV
200ms
I_sust
I_Inst
10ms
B
I_Inst
I_sust
I_H=I_sust-I_inst
I_max
5
4
3
2
1
0
n.s.
n.s.
n.s.
7
7
7
7
7
7
control
~20min
control
~20min
control
~20min
C
G/G_max
1.0
0.75
0.5
0.25
0
control
10min
20min
25min
-120
-100
-80
-60
Voltage (mV)
D
V_1/2 (mV)
-120
-100
-80
-60
n.s.
7
7
control
~20min

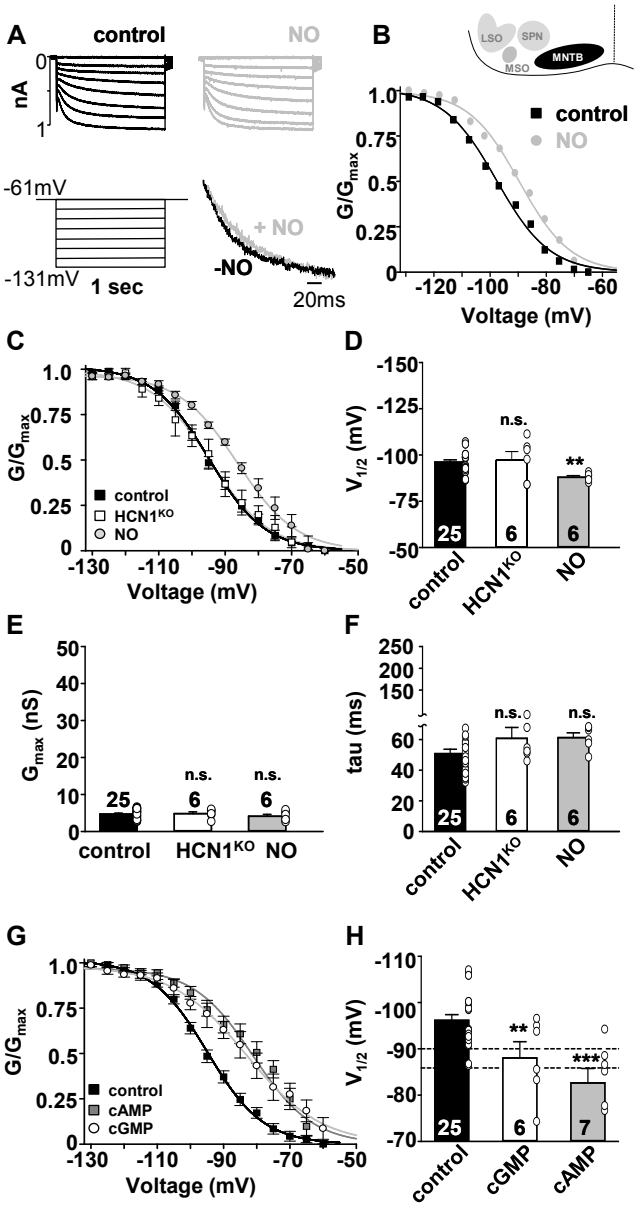
A
control
NO
0
nA
1
-61mV
-131mV
1 sec
+ NO
-NO
20ms
B
LSO
SPN
MSO
MNTB
control
NO
G/Gmax
Voltage (mV)
C
control
HCN1KO
NO
G/Gmax
Voltage (mV)
D
V1/2 (mV)
n.s.
**
25
6
6
control
HCN1KO
NO
E
Gmax (nS)
n.s.
n.s.
25
6
6
control
HCN1KO
NO
F
tau (ms)
n.s.
n.s.
25
6
6
control
HCN1KO
NO
G
control
cAMP
cGMP
G/Gmax
Voltage (mV)
H
V1/2 (mV)
**
***
25
6
7
control
cGMP
cAMP

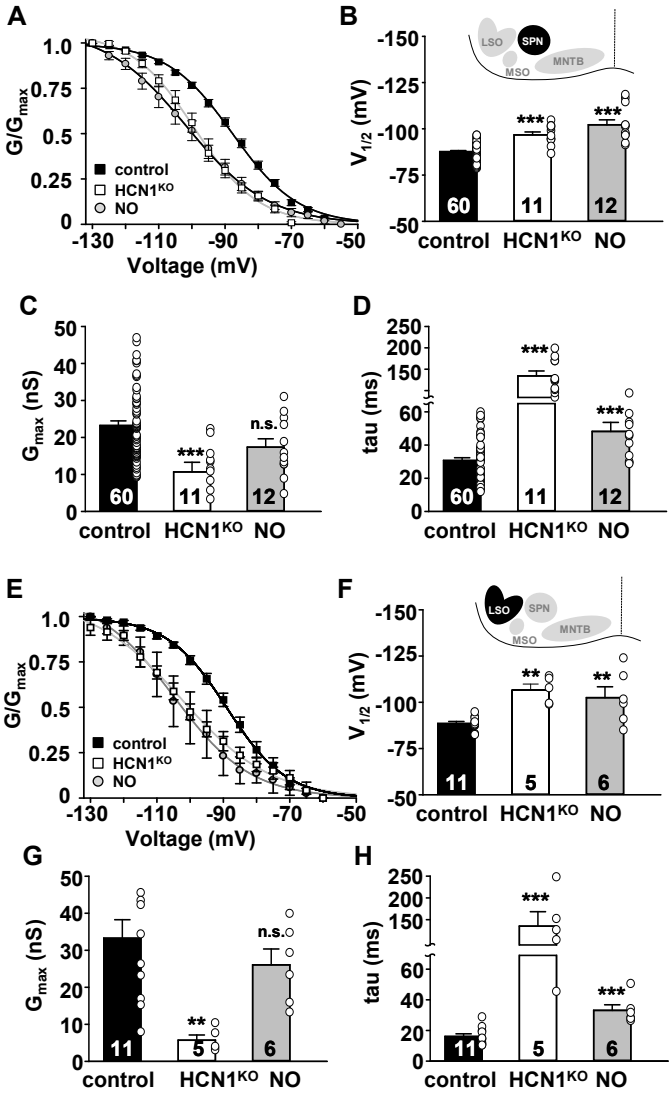
A
B
C
D
E
F
G
H
control
HCN1KO
NO
Voltage (mV)
G/Gmax
Gmax (nS)
V1/2 (mV)
tau (ms)
LSO
SPN
MNTB
MSO
n.s.
***
**
60
11
12
5
6

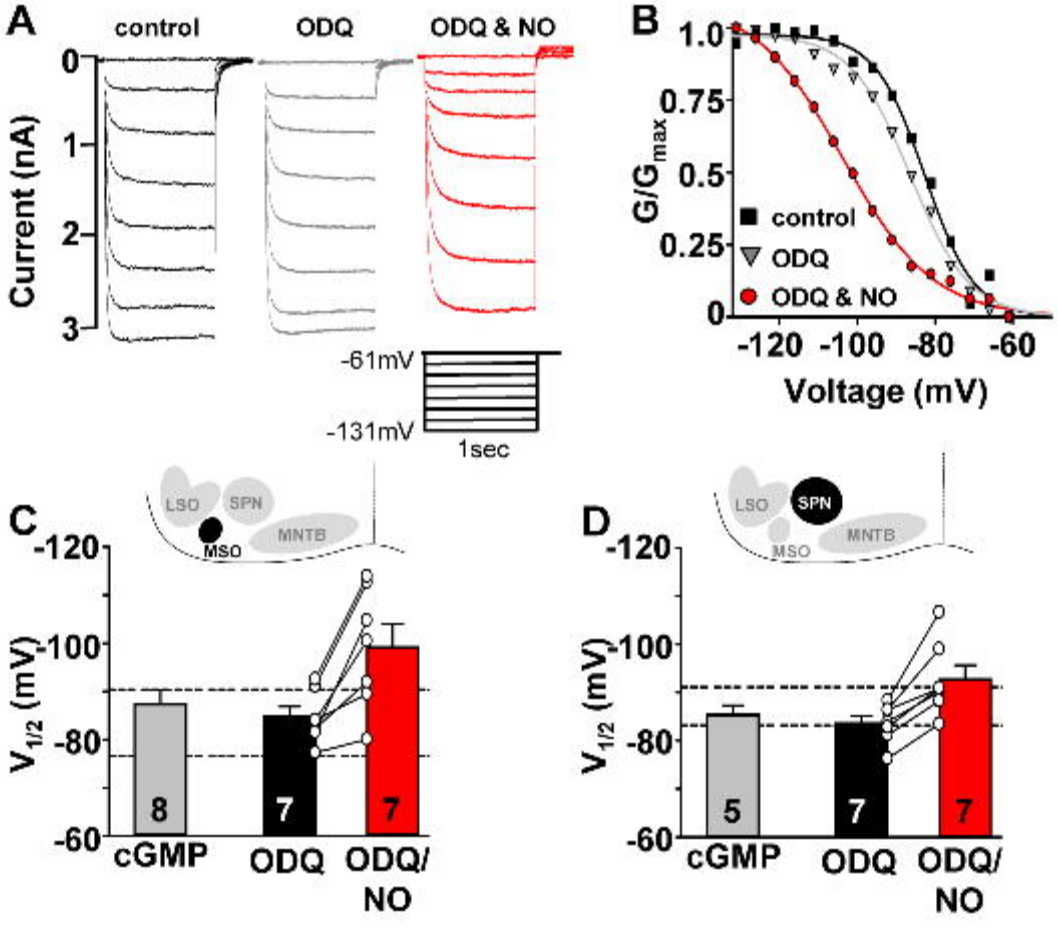
A
control
ODQ
ODQ & NO
Current (nA)
0
1
2
3
-61mV
-131mV
1sec
B
G/G_max
1.0
0.75
0.5
0.25
0
control
ODQ
ODQ & NO
-120
-100
-80
-60
Voltage (mV)
C
LSO
SPN
MSO
MNTB
V1/2 (mV)
-120
-100
-80
-60
8
7
7
cGMP
ODQ
ODQ/ NO
D
LSO
SPN
MSO
MNTB
V1/2 (mV)
-120
-100
-80
-60
5
7
7
cGMP
ODQ
ODQ/ NO

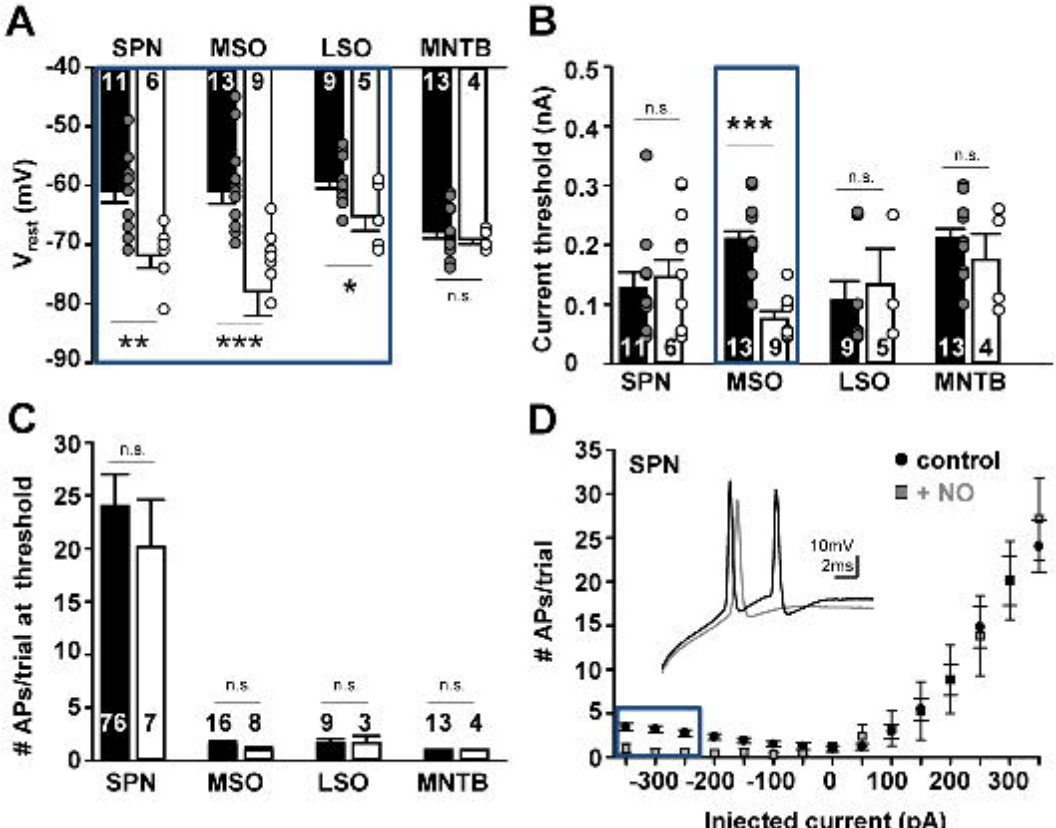
A
SPN
MSO
LSO
MNTB
V_{rest} (mV)
-40
-50
-60
-70
-80
-90
11
6
13
9
9
5
13
4
**
***
*
n.s.
B
Current threshold (nA)
0.5
0.4
0.3
0.2
0.1
0
n.s.
***
n.s.
n.s.
11
6
13
9
9
5
13
4
SPN
MSO
LSO
MNTB
C
APs/trial at threshold
30
25
20
15
10
5
0
n.s.
n.s.
n.s.
n.s.
76
7
16
8
9
3
13
4
SPN
MSO
LSO
MNTB
D
SPN
control
+ NO
10mV
2ms
APs/trial
35
30
25
20
15
10
5
0
-300
-200
-100
0
100
200
300
Injected current (pA)